

Microwave Focusing with Temporal Interference for Non-Invasive Deep Brain Stimulation

Mika Söderström, Melker Carlsson, Patrik Nicolausson, and Mariana Dalarsson

Abstract—Deep Brain Stimulation (DBS) is effective in treating neurological disorders but involves invasive surgery. Non-invasive DBS aims to overcome surgical risks by means of externally applied electromagnetic fields. In this work, we present a method for non-invasive microwave focusing of amplitude-modulated electric fields in the human brain using an external antenna array. The method combines iterative time-reversal (iTR) and genetic-algorithm-based temporal interference (TI) optimization to determine antenna positions, orientations, operating frequency, amplitudes, and phases of each element. Magnetic point dipoles are used as idealized radiative sources, providing a design-independent benchmark for optimization studies. Furthermore, this work incorporates realistic tissue properties from voxelized anatomical head models, accounting for variations in permittivity and conductivity. The iTR algorithm provides an initial antenna configuration that serves as a reliable starting point for the subsequent TI optimization, improving convergence and focusing precision. The results demonstrate that amplitude-modulated electromagnetic fields can be selectively and precisely shaped within predefined focal regions. Thereby, this study demonstrates a proof-of-principle of non-invasive microwave field focusing using iTR and TI in a realistic human head model.

Index Terms—antenna array optimization, computational modeling, deep brain stimulation, iterative time reversal, microwave focusing, neural stimulation, non-invasive, temporal interference, voxel head model

I. INTRODUCTION

DEEP Brain Stimulation (DBS) is a medical treatment method for neurological disorders, including movement disorders such as Parkinson’s disease [1], [2], epilepsy [3], and depression [4]. The method modulates neurons in targeted regions of the brain [5], [6], to neutralize abnormal neural oscillations that are linked to neurological disorders [7]. In general, the primary targets for DBS are deep brain structures, rather than the outermost layer of the brain [8].

Deep brain stimulation is currently achieved using electrodes implanted in the brain, as seen in Fig. 1. This is an invasive treatment that delivers electrical stimulation directly to the targeted neural tissue [9], at frequencies around 100 Hz [10]. However, this invasive approach carries risks including

hemorrhagic stroke [11], surgical complications, infections, and tissue reactions such as inflammation and gliosis, that can alter long-term stimulation efficacy. Other technological issues include hardware failure, limited battery life, and electromagnetic interference or heating during magnetic resonance imaging (MRI) scans [5]. As a result, non-invasive treatments are being proposed to overcome the need for implantable electrodes.

Non-invasive methods are based on using external sources to induce electromagnetic (EM) fields within the brain to achieve neural stimulation. The commonly studied non-invasive methods are transcranial magnetic stimulation (TMS) [12], [13] and transcranial electric stimulation (TES) [14], using low-frequency fields in the kHz frequency range.

While low-frequency fields can penetrate the skull in both TMS and TES, they lack the spatial precision required to selectively target specific deep brain regions. Therefore, high-frequency fields in the microwave (MW) range have been proposed due to their potential to achieve greater spatial focusing [15]. The long-term goal of this innovative stimulation method using MW fields is to provide patients with the same, or improved, therapeutic benefits as the clinically accepted invasive DBS, without the associated risks.

Microwave-based systems have been explored in medical applications as a non-ionizing alternative to conventional methods for diagnostics and therapy [16]. External MW arrays have been proposed for head imaging, including the detection of brain tissue damage such as stroke [17]–[20] and tumours [21], as well as for therapeutic applications such as MW hyperthermia for cancer treatment [22]–[25]. Microwaves are also being investigated for brain stimulation, both invasive and non-invasive, where a wide-ranging review is provided in [26]. The extensive research on MW systems in medical imaging and hyperthermia, together with the insights provided in [26], makes external MW array antenna systems emerge as a promising approach to achieve focused electric fields for non-invasive DBS, see Fig. 2.

In general, electrical neuromodulation is not achievable at high frequencies due to the neuron’s ability to low-pass filter electrical signals [27], with cut-off frequencies typically below 1 kHz [28], far lower than the radio- or microwave frequency range. However, Temporal Interference (TI) could overcome this limitation by combining two high-frequency signals, and thereby generate a low-frequency envelope that can stimulate neurons [29]. By steering the maxima of this envelope, stimulation can be targeted to specific regions inside the head. Since neurons do not respond to the high-frequency components, the TI fields can pass through outer brain regions without inducing unintended stimulation [9]. Consequently,

This work was supported by the Swedish Research Council, project number 2023-04887, and by the Göran Gustafsson foundation, 2406.

M. S. is with the Department of Electromagnetics and Plasma Physics, KTH Royal Institute of Technology, 100 44 Stockholm, Sweden (e-mail: mikaso@kth.se).

M. C. is with the Department of Electromagnetics and Plasma Physics, KTH Royal Institute of Technology, 100 44 Stockholm, Sweden (e-mail: melker@kth.se).

P. N. is with the Department of Electromagnetics and Plasma Physics, KTH Royal Institute of Technology, 100 44 Stockholm, Sweden (e-mail: pnica@kth.se).

M. D. is with the Department of Electromagnetics and Plasma Physics, KTH Royal Institute of Technology, 100 44 Stockholm, Sweden (e-mail: mardal@kth.se).

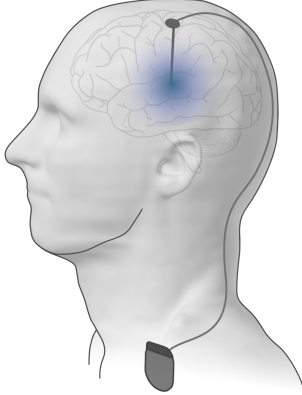


Fig. 1. Conceptual illustration of the clinically accepted invasive DBS treatment, with implanted electrodes that deliver electric fields to induce neural stimulation in a target region. The electrodes are connected to a pulse generator via leads.

combining MW focusing and TI techniques for an external MW antenna array could enable targeted neural stimulation, while reducing both off-target stimulation and undesired tissue heating.

In practice, realizing such selective stimulation depends on accurately predicting the spatial distribution of the resulting electromagnetic fields inside the head. This task is non-trivial since EM wave propagation is strongly influenced by heterogeneous tissues, complex anatomical geometries, and frequency-dependent material properties. These challenges motivate the use of computational models to analyse and optimize non-invasive DBS systems.

Computational models of DBS can be classified across multiple levels of abstraction, including EM field modeling (macro-scale), network modeling (meso-scale), and neuro-physiological modeling (micro-scale) [12]. In this work, we focus on EM field modeling, where the goal is to optimize a microwave antenna array to achieve precise electric field focusing within a target brain region. Solving these problems accurately is challenging due to the heterogeneous nature of brain tissue and sharp tissue interfaces, giving rise to complex internal reflections.

Previous MW-DBS studies have largely relied on simplified EM and head models. In [30], analytical equations were derived for electromagnetic focusing in a homogeneous, lossless hemispherical head model with a large number of fixed antennas distributed over two hemispheres. Numerical calculation of individual antenna-element Green's functions was introduced in [15] for a three-layer spherical head model, with joint optimization of excitation phases and amplitudes for magnetic dipole elements. Full-wave electromagnetic simulations using Hertzian dipoles and a homogeneous three-dimensional head model with averaged dielectric properties were employed in [31]. A more anatomically detailed representation was considered in [32], which used a coarse three-dimensional voxel head model comprising five tissue types and a cylindrically arranged dipole array. Despite their contributions, these studies

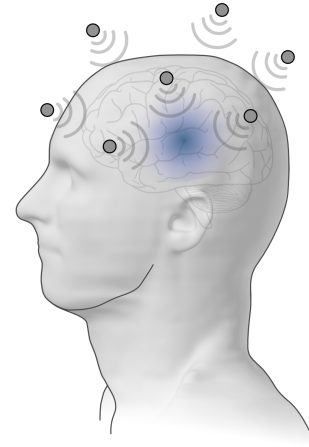


Fig. 2. Conceptual illustration of the proposed non-invasive DBS treatment, where an external microwave antenna array delivers focused electric fields to induce neural stimulation in a target brain region.

lack realism in several respects. In particular, they do not fully capture tissue heterogeneity in the human head, both in terms of the number of tissue types and their spatial variation. Furthermore, the use of high operating frequencies raises concerns regarding field penetration depth, and the reliance on large numbers of antenna elements may limit practical feasibility. These MW-DBS studies do not consider TI-based stimulation, and instead investigate single-frequency MW field focusing without addressing the neuronal stimulation mechanism. These limitations highlight the need for more medically realistic simulation frameworks that account not only for anatomical and electromagnetic complexity, but also their relevance to neuronal stimulation. Although MW-DBS research is still in its early stages, insights from microwave hyperthermia treatment methodologies, combined with established TI concepts, can provide a valuable foundation for developing more comprehensive and physically realistic models for non-invasive DBS.

The setup for MW-DBS will be similar to that used in MW hyperthermia treatments, with an antenna array positioned in a matching medium to reduce reflections and improve field transmission into the head [33]. Achieving precise field focusing in such heterogeneous tissue requires solving complex EM wave propagation problems involving heterogeneous, lossy, and dispersive media, which can be effectively addressed using optimization algorithms. Heuristic approaches, such as Particle Swarm Optimization (PSO) [24], [34] and Genetic Algorithms (GA) [35], can be employed to determine the optimal antenna excitations, including orientation, amplitude, and phase.

Optimization algorithms often involve a large number of variables and computationally expensive iterations, particularly in heterogeneous, lossy and dispersive human tissue models. To improve convergence and reduce computational cost, it is advantageous to provide a physically informed initial guess. Electromagnetic time reversal (TR) is a well-established method for focusing EM fields in biological tissue [22], [32], [36], [37]. In TR, a virtual source is placed at the desired focal point, the impulse response is recorded at potential

antenna positions, and then back-propagated to recreate the field of the virtual source [38]. Thus, the resulting TR-based antenna excitation parameters can serve as starting values for subsequent optimization, enabling the solution to be refined more efficiently. This ultimately allows for control and steering of the EM field focus to minimize unwanted interference and maximise stimulation effectiveness [26].

In this work, we present a non-invasive MW-DBS framework for spatial electric field focusing and TI-based neural stimulation. The framework is based on an advanced MRI-based voxel head model that captures detailed tissue heterogeneity and electromagnetic losses in the human head [39]. The proposed approach utilises an external antenna array of magnetic point dipoles (MPDs) together with iTR, inspired by [22], to determine the optimal physical placement and orientation of antennas. The resulting iTR steering parameters then serve as initial values for TI optimization, enabling precise targeting of neural stimulation. The stimulation method is based on temporal interference between two high-frequency fields, producing a low-frequency amplitude-modulated envelope that is localized to the target region and suppressed elsewhere. This proof-of-principle study demonstrates a general and robust framework that can accommodate different antenna configurations, optimization parameters, and objective functions. At the same time, the framework explicitly addresses anatomical realism in the head model and relevance to neural stimulation through TI. To the best of the authors' knowledge, this is the first study to combine iterative time reversal and temporal interference optimization within a realistic voxel-based head model for non-invasive DBS.

II. METHODOLOGY

To achieve selective neural stimulation, we employ a two-stage methodology. First, iTR is used to optimize antenna placement, determining the positions, orientations, and initial steering parameters of the antenna elements, see Fig. 3. Second, TI optimization refines amplitude, phase, and frequency assignment of each element to maximize the envelope amplitude within the focal region. All field computations are carried out using COMSOL Multiphysics® [40], with optimization performed in MATLAB® [41].

A. Iterative Time Reversal

1) *Classical Time Reversal*: Mathematically, the TR operator, denoted as Γ , reverses the direction of time in the field expressions in the time domain according to

$$\begin{cases} \Gamma\{\mathbf{E}(\mathbf{r}, t)\} = \mathbf{E}(\mathbf{r}, -t) \\ \Gamma\{\mathbf{H}(\mathbf{r}, t)\} = -\mathbf{H}(\mathbf{r}, -t). \end{cases} \quad (1)$$

In the frequency domain, using the time convention $e^{j\omega t}$, TR corresponds to taking the complex conjugate of the Fourier transformed field

$$\begin{cases} \Gamma\{\mathbf{E}(\mathbf{r}, \omega)\} = \mathbf{E}^*(\mathbf{r}, \omega) \\ \Gamma\{\mathbf{H}(\mathbf{r}, \omega)\} = -\mathbf{H}^*(\mathbf{r}, \omega). \end{cases} \quad (2)$$

Within an enclosed surface, the EM field can be reconstructed anywhere inside the volume by placing infinitesimal sources

on the enclosing surface [42], in accordance with Huygens' principle.

Although ideally reconstructed over a continuous surface, the field is in practice reconstructed only at discrete locations. To reconstruct the magnetic field at a specific point \mathbf{r}' , a magnetic dipole \mathbf{m} can be placed at that location, with its steering parameters defined by the computed \mathbf{H} -field as

$$\mathbf{m}(\mathbf{r}') = -\eta \mathbf{H}^*(\mathbf{r}') \quad (3)$$

where $\eta = \sqrt{\mu\varepsilon^{-1}}$ is the wave impedance [38]. When all radiating sources lie within the same domain, η is constant for all elements and acts only as a scaling factor. This principle underlies TR methods, where antenna positions and steering parameters are optimized using an iterative process to maximize field strength at a target location.

2) *Forward Field*: In this work, a point source is first placed at the desired focal point \mathbf{r}_f inside the head, and the forward field is computed using the full-wave solver COMSOL. Since COMSOL does not provide an ideal point source, the excitation is approximated using three electric point dipoles

$$\mathbf{p}_k = p_k \hat{\mathbf{p}}_k e^{j\alpha_k} \quad (4)$$

oriented along the Cartesian unit vectors $\hat{\mathbf{p}}_k \in \{\hat{\mathbf{x}}, \hat{\mathbf{y}}, \hat{\mathbf{z}}\}$, with p_k being the amplitude and α_k the phase. The index $k \in \{x, y, z\}$ is attributed to the electric dipoles of the point source generating the forward field. The total forward field is obtained by summing the fields generated by each dipole $\mathbf{H} = \mathbf{H}_x + \mathbf{H}_y + \mathbf{H}_z$.

3) *Backward Field*: The complex conjugate of the forward field, referred to as the backward field, is then evaluated at the candidate antenna positions \mathbf{r}_n and used to determine the antenna elements \mathbf{m}_n . Here, the index n is attributed to the antenna elements, the magnetic dipoles, of the external array. Each element is characterized by its magnitude m_n , direction $\hat{\mathbf{m}}_n$ and phase α_n according to

$$\mathbf{m}_n = m_n \hat{\mathbf{m}}_n e^{j\alpha_n}. \quad (5)$$

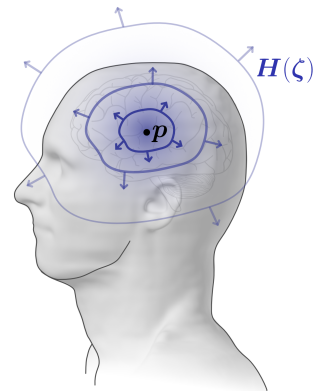


Fig. 3. Conceptual illustration of the TR-based field focusing method. A point source \mathbf{p} is placed inside the head generating a forward magnetic field $\mathbf{H}(\zeta)$, which is dependent on the optimization parameters in ζ .

The TR algorithm seeks to minimize the following objective function

$$\mathcal{J}_{\text{TR}} = \sum_i \sum_n w(\mathbf{r}_i, \mathbf{r}_n) |\mathbf{m}_n - \beta(\mathbf{r}_n, \mathbf{r}_f)^b \mathbf{H}^*(\mathbf{r}_n)|^2 \quad (6)$$

where \mathbf{m}_n are the selected dipoles at positions \mathbf{r}_n , \mathbf{r}_i are the observation points, and $w(\mathbf{r}_i, \mathbf{r}_n)$ a sampling weight. The factor $\beta(\mathbf{r}_n, \mathbf{r}_f)$ is an attenuation compensation factor and represents the inverse of the expected attenuation along a straight path between the candidate dipole position \mathbf{r}_n and focus point \mathbf{r}_f . It is defined as

$$\beta(\mathbf{r}_n, \mathbf{r}_f) = \exp\left\{\int_{\mathbf{r}_n}^{\mathbf{r}_f} \alpha(\mathbf{r}) \, d\ell\right\} \quad (7)$$

where the local attenuation constant $\alpha(\mathbf{r})$ is given by

$$\alpha(\mathbf{r}) = \omega \sqrt{\frac{\mu_0 \varepsilon_0}{2}} \sqrt{|\varepsilon(\mathbf{r})| - \Re\{\varepsilon(\mathbf{r})\}} \quad (8)$$

which represents a high-frequency approximation of the local attenuation in a lossy dielectric medium. The exponent $b \in [0, 1]$ in Eq. (6) is introduced to control the degree of attenuation compensation applied through β^b . Selecting b within this range therefore allows a balanced, partial correction for tissue losses while avoiding large weighting of distant or heavily attenuated dipoles. The sampling function $w(\mathbf{r}_i, \mathbf{r}_n)$ is a Gaussian function, decaying with distance from the antenna position according to

$$w(\mathbf{r}_i, \mathbf{r}_n) = \exp\left\{-\frac{|\mathbf{r}_i - \mathbf{r}_n|^2}{2\sigma^2}\right\} \quad (9)$$

where σ is the standard deviation of the Gaussian weighting function used to evaluate the local field around each candidate dipole.

4) *Iterative Time Reversal*: A single TR solution may produce an asymmetric or poorly confined focal region due to the strongly heterogeneous and lossy structure of the human brain. To address this, the point source steering parameters and the attenuation-compensation exponent b are updated iteratively. In each iteration, a forward field is computed, a backward field is reconstructed, and the parameter set

$$\zeta = [\{p_k\}_k, \{\alpha_k\}_k, b] \quad (10)$$

are optimized using Bayesian optimization in MATLAB® [43] to obtain a backward field that best approximates the ideal TR field. To formalize this optimization, we define the iTR objective function for the backward field as

$$\mathcal{J}_{\text{iTR}} = c_1 \text{HIR} + c_2 \text{FIQ} \quad (11)$$

with positive weights c_1 and c_2 . The iTR objective function is formulated in terms of the electric field since neuronal stimulation is determined by the local electric field rather than the magnetic field. The half-intensity radius (HIR) is the smallest radius for which the spherical average of the intensity of the electric field

$$I(\mathbf{r}) = \|\mathbf{E}(\mathbf{r})\|^2 \quad (12)$$

falls below half of its value at the focal point. Here,

$$\|\mathbf{E}(\mathbf{r})\| = \sqrt{|E_x(\mathbf{r})|^2 + |E_y(\mathbf{r})|^2 + |E_z(\mathbf{r})|^2} \quad (13)$$

denotes the electric field magnitude. The focus intensity quotient (FIQ) evaluates field confinement and is defined as

$$\text{FIQ} = \frac{\overline{I(\mathbf{r})}_{\Omega_b}}{\overline{I(\mathbf{r})}_{\Omega_f}} \quad (14)$$

where Ω_f is the focal region and Ω_b is the background region. The objective function (11) therefore promotes a narrow focal region while minimizing unintended field levels elsewhere.

The iterative TR algorithm is illustrated in Fig. 4 and can be summarised as follows

(i) **Calculate the forward field**

Calculate the forward field $\mathbf{H}_k(\mathbf{r})$ generated by each electric point dipole \mathbf{p}_k , $k \in \{x, y, z\}$ placed at the focal location \mathbf{r}_f .

(ii) **Rank candidate antenna positions**

For each candidate position \mathbf{r}_n , compute the local weighted energy

$$W = \sum_i w(\mathbf{r}_i, \mathbf{r}_n) |\beta(\mathbf{r}_n, \mathbf{r}_f) \mathbf{H}^*(\mathbf{r}_i)|^2 \quad (15)$$

and sort positions in descending order of W .

(iii) **Select a feasible antenna position**

Select the highest-ranked candidate \mathbf{r}_n that satisfies the minimum inter-element spacing constraint d_{\min} . Remove this position from the candidate list.

(iv) **Optimize the dipole at the selected position**

For the chosen position \mathbf{r}_n , determine the parameters $m_n, \hat{\mathbf{m}}_n, \alpha_n$ that minimizes the objective function \mathcal{J}_{TR} , given by Eq. (6).

(v) **Repeat position and parameter selection**

Repeat steps (iii)-(iv) until either the maximum number of antenna elements N_{\max} is reached, or no additional candidates satisfy the spacing constraint.

(vi) **Evaluate the backward field**

For the selected $N \leq N_{\max}$ dipoles $\{\mathbf{m}_n\}_{n=1}^N$ at positions $\{\mathbf{r}_n\}_{n=1}^N$, compute the resulting backward field and evaluate the iTR objective \mathcal{J}_{iTR} , given by Eq. (11). If improved, store the current array as the best configuration to date.

(vii) **Update TR parameters**

Adjust the TR point source parameters ζ and recompute the forward field accordingly.

(viii) **Iterate until convergence**

Repeat steps (ii)-(vii) until the objective meets the desired threshold or the maximum number of iterations is reached.

The proposed method extends iTR approach developed in [24] by directly evaluating the full vector field at each TR iteration, without relying on pre-computed fields or virtual sources. Consistent with [42], the method assumes that the time-reversed fields ideally form a continuous enclosing surface,

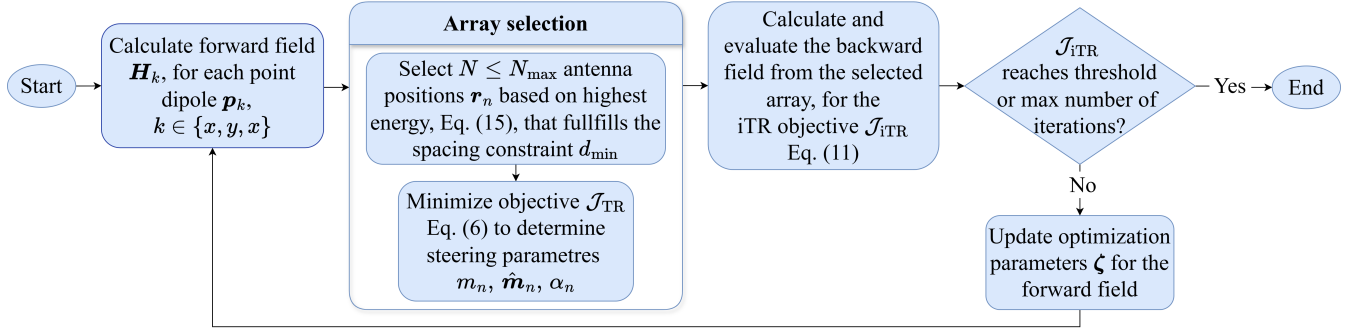


Fig. 4. Flowchart showing the implemented iTR optimization.

with the discrete sources serving as a practical approximation. This framework provides an efficient and accurate method to achieve field focusing around the target.

B. Temporal Interference

The neural stimulation mechanism underlying TI was first proposed by Grossman *et al.* [29], who hypothesized that neurons demodulate amplitude-modulated signals, responding to the low-frequency envelope rather than the high-frequency carrier. The amplitude-modulated field is obtained by combining two electric fields

$$\mathbf{E}_{\text{TI}} = \mathbf{E}_{f_1} + \mathbf{E}_{f_2} \quad (16)$$

where \mathbf{E}_{f_1} and \mathbf{E}_{f_2} denote the fields generated at frequencies f_1 and $f_2 = f_1 + \Delta f$, respectively. Their superposition produces an amplitude-modulated field whose envelope oscillates at the difference frequency Δf . This principle is illustrated in Fig. 5.

Under this TI hypothesis, neuronal activation is expected to occur in regions where the modulation depth of the electric field is maximal. The envelope amplitude at a point \mathbf{r} , as defined in [44], is given by

$$E_{\text{AM}}(\mathbf{r}) = 2 \min(\|\mathbf{E}_{f_1}(\mathbf{r})\|, \|\mathbf{E}_{f_2}(\mathbf{r})\|) \quad (17)$$

where each field norm is calculated using Eq. (13). This low-frequency envelope is believed to drive neuronal modulation even when the carrier frequencies lie in the MHz or GHz frequency range [45]–[47]. Thus, maximizing the envelope amplitude (17) within the focal region is a central objective in TI field optimization.

A common optimization method for determining steering parameters in MW-focusing inside human tissues is Particle Swarm Optimization (PSO), particularly in Hyperthermia treatment planning [24], [34]. Genetic Algorithm (GA) has also been applied for optimizing antenna feed parameters [35]. An advantage of GA for this application is its inherent support for mixed-integer optimization [48], allowing the algorithm to assign each antenna element to either frequency f_1 or f_2 . This effectively provides an element-wise on/off selection for each frequency, which is essential for generating the desired temporal interference pattern.

After obtaining an optimized array geometry from the iTR algorithm, the antenna positions \mathbf{r}_n and orientations $\hat{\mathbf{m}}_n$ are

fixed. The magnitudes m_n and phases α_n are then used as initial values for the TI optimization. Each antenna element is assigned one of the two operating frequencies f_1 or f_2 , and its amplitude and phase at the assigned frequency are independently adjustable, denoted as m_{n_i} and α_{n_i} , where $i \in \{1, 2\}$ indicates the frequency index. The resulting electric field contribution from element n_i at frequency f_i is described by its Green's function \mathbf{G}_{n_i} , obtained by simulating each element individually. The total electric field at frequency f_i is

$$\mathbf{E}_{f_i} = \sum_{n_i=1}^{N_i} \mathbf{G}_{n_i}(f_i) m_{n_i} e^{j\alpha_{n_i}}. \quad (18)$$

Here, N_i is the number of elements assigned to frequency f_i . Each $\mathbf{G}_{n_i} \in \mathbb{C}^3$ contains the three Cartesian field components and is linear with respect to amplitude and phase, making it suitable for frequency-domain optimization [15], [44], [49], [50].

To localize the TI envelope at the target region, the optimization minimizes the following objective function

$$\mathcal{J}_{\text{TI}} = \frac{\overline{E_{\text{AM}}(\mathbf{r})}_{\Omega_b}}{\overline{E_{\text{AM}}(\mathbf{r})}_{\Omega_f}} \quad (19)$$

which measures the ratio of the average TI modulation depth in the background region Ω_b to that in the focal region Ω_f .

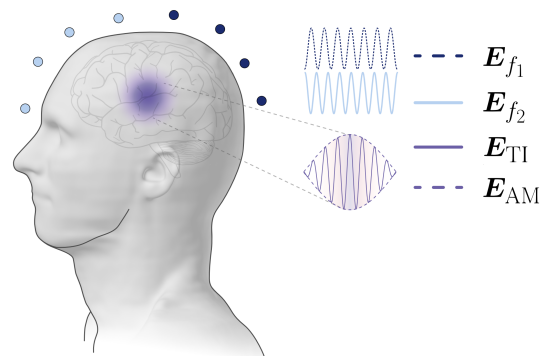


Fig. 5. Conceptual illustration of TI-based non-invasive DBS. Two high frequency fields, \mathbf{E}_{f_1} and \mathbf{E}_{f_2} , interfere to produce an amplitude-modulated field $\mathbf{E}_{\text{TI}} = \mathbf{E}_{f_1} + \mathbf{E}_{f_2}$, resulting in a low-frequency envelope E_{AM} .

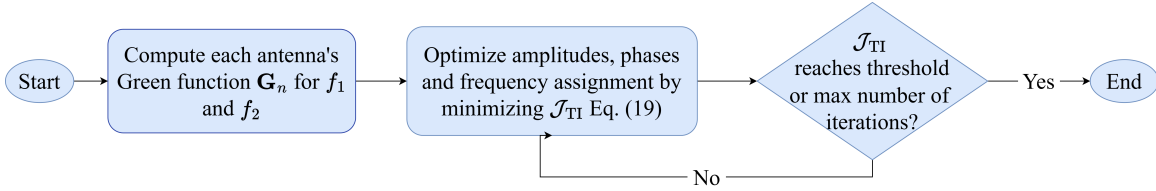


Fig. 6. Flowchart showing the implemented TI optimization.

Minimizing \mathcal{J}_{TI} concentrates the spatial localization of the TI envelope by concentrating modulation energy in the target while suppressing it elsewhere. Since high modulation depth requires both large and balanced field amplitudes from f_1 and f_2 , the objective is sensitive to both relative and absolute field strengths.

The TI algorithm is illustrated in Fig. 6 and can be summarised as follows

- (i) **Import the iTR-derived antenna geometry**
Use the antenna array geometry produced by the iTR algorithm, from which we obtained fixed positions and orientations.
- (ii) **Compute frequency-specific Green's functions**
For each antenna element $n = 1, \dots, N$, compute the Green's functions through individual element simulations in COMSOL at frequency f_1 .
- (iii) Repeat step (ii) for f_2 .
- (iv) **Optimize amplitudes, phases, and frequency assignment**
Use the full set of Green's functions obtained in step (ii) and (iii), and apply GA to optimize
 - a) frequency assignment, f_1 or f_2 of each element, and
 - b) amplitude m_{n_i} and phase α_{n_i} at the chosen frequency by minimizing the objective function \mathcal{J}_{TI} , given by Eq. (19).
- (v) **Evaluate TI objective and iterate until convergence**
If the objective improves, the configuration is stored. GA iterations continue until the objective meets the desired threshold or the maximum number of iterations is reached.

In practice, GA outperforms PSO in both runtime and final objective values. This is likely due to GA's native support for discrete variables, whereas MATLAB's PSO implementation only handles continuous variables, requiring binary decisions to be approximated by rounding. Such rounding introduces discontinuities that degrade PSO's performance by producing non-smooth or non-informative objective landscapes.

III. SIMULATION ENVIRONMENT

A human head model was placed inside a spherical domain with a scattering boundary condition on its outer surface. Magnetic dipole antennas were positioned around the head, and a matching layer was added to minimize reflections from the radiating antennas. This matching layer extended between the head model and the scattering boundary. Simulations were

carried out for operating frequencies in the range of 400 MHz to 1 GHz.

A. Anatomical Head Model

The human head is highly inhomogeneous and anisotropic, consisting of numerous anatomical structures and tissue types with a great variation in dielectric properties. This complexity makes accurate electromagnetic modeling particularly demanding. Voxelized anatomical models address this challenge by providing detailed, spatially resolved representations of biological tissues. Among these, the IT'IS Foundation models [51] are widely used and well validated in bioelectromagnetic research, enabling reproducible and comparable studies across the field. In the present work, we used the anatomical head model from Duke, who is a member of the IT'IS Virtual Population [39].

For our simulations, we isolated the head by cutting the full-body model at a height of $z_{\text{cut}} = 1.6$ m. In this voxelized model, the total voxel count increases rapidly with finer voxel sizes. To balance computational cost and spatial resolution, the 2 mm voxel model was selected. A voxel-based NASTRAN mesh was then generated and imported into COMSOL to define the full three-dimensional head geometry.

For material characterization, each voxel was assigned one of the 77 tissue labels defined in the full-body model. Dielectric properties for all tissues are obtained from the IT'IS Tissue Database [52], which provides Cole–Cole parameters to describe the frequency-dependent permittivity of biological tissues, assuming isotropic behaviour. Fig. 7 illustrates the resulting permittivity distribution in a central slice through the head.

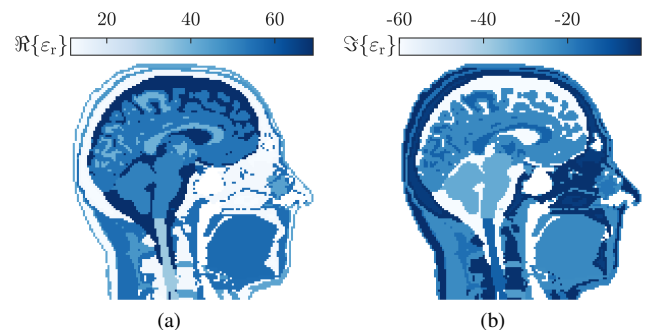


Fig. 7. (a) Real, and (b) imaginary part of the relative permittivity ϵ_r of the tissues in the voxelized Duke head model, for a voxel size of 2 mm.

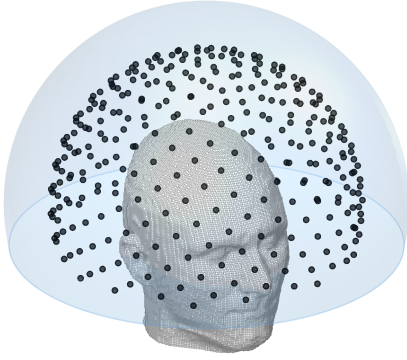


Fig. 8. Voxelized Duke head model surrounded by a matching layer in light blue. The dots indicate all candidate antenna positions r_i for the array before iTR optimization.

B. Antenna Array

Magnetic point dipoles (MPDs) were used to model the antenna elements. Practical antenna design will ultimately need to be integrated into the optimization framework for medical applications. This poses a challenge because antenna behaviour in the reactive near field of highly heterogeneous tissues, such as the human head, is poorly characterized. MPDs, however, provide a reliable and well-understood source model that is independent of specific antenna geometries. This makes them suitable as a benchmark for optimization studies.

A lossless matching layer with permittivity $\epsilon_{ml} = 40$ was introduced, in which the antennas are placed. The matching layer does not fully enclose the head but is cut above the nose, leaving air below. This design reflects a more realistic scenario where the matching layer cannot cover the mouth or nose, see Fig. 8.

Candidate antenna positions r_i for the iTR optimization were positioned within the matching layer on a Fibonacci sphere, centered around the head, as seen in Fig. 8. Approximately 300 candidate positions were used for all results in this study. A minimum spacing of d_{min} was imposed between dipoles to ensure physical realizability, prevent excessive electromagnetic coupling, and avoid clustering of elements on one side (e.g., for lateral focus points). This enforces practical design constraints and promotes a uniform distribution of antenna elements.

The iTR optimization was performed using the candidate antenna locations r_i on the Fibonacci sphere, a minimum constraint $d_{min} = 6$ cm, and a maximum number of antennas $N_{max} = 35$. The Gaussian weight width was set to $\sigma = \frac{0.8}{3} d_{min}$, making the sampling window $w(\mathbf{r})$ effectively negligible beyond $3\sigma = 0.8d_{min}$. Given that d_{min} is the minimum spacing between antenna elements, the Gaussian windows of neighbouring antennas have minimal overlap. The focal region Ω_f was defined as a sphere of radius 1 cm, centered around the focus point r_f . The background region Ω_b was the rest of the head, excluding the focal region. With these settings, the optimization resulted in arrays of between 33 and 35 elements, depending on the focal point location.

IV. RESULTS

Results are presented for the frequency 700 MHz for iTR, and $f_1 = 700$ MHz and $f_2 = f_1 + 100$ Hz for TI. These frequencies provide a favourable trade-off between sufficiently narrow focality and minimal field absorption in human tissue. We have chosen a center focus point at the center of Duke's head at a height of 175 cm and side focus by shifting r_f with 2 cm to the side towards the right ear.

To visualize the fields, we follow standard medical imaging conventions, extracting three orthogonal anatomical planes: sagittal, coronal and axial, corresponding to dividing the body into left/right, front/back, and upper/lower, sections [53]. The intersection of these planes is placed at the location of the maximum field observed within the desired focal region.

As the exact field strengths required to stimulate neurons at MW frequencies remain uncertain, we present normalized results. Values are normalized to the maximum within the focal region of the quantity of interest, either the field magnitude $\|\mathbf{E}\|$ for iTR or the envelope amplitude $|E_{AM}|$ for TI. This approach allows for clear visualization of how the fields form within the heterogeneous head.

A. Iterative Time Reversal

The properties of the iTR-generated array, for center focus, are presented in Fig. 9. In all three Figs. 9(a)–(c), we can see the position of each MPD along with their respective directions in (a), normalized magnitudes in (b), and phases in (c).

The results of the normalized electric field norm after iTR optimization are shown in Fig. 10 for center focus and in Fig. 11 for side focus. The field is observed to be focused either at the center or toward the side of the brain, as intended. It can also be seen that the field builds up in certain parts of the head due to the inhomogeneous head structure with highly varying permittivity. This is also commonly observed in MW hyperthermia focusing [24], [54].

B. Temporal Interference

The frequency assignment obtained after the TI optimization is shown in Fig. 12 for both the center and side focus. For the center focus array in Fig. 12(a), the antennas are split evenly between the two operating frequencies, f_1 and f_2 , and the distribution is approximately symmetric across the left and right sides of the head. For the side focus configuration in Fig. 12(b), there is no longer an even split between the two frequencies, and the assignment is noticeably asymmetric. The TI optimization assigns the frequency f_1 to the antennas located closer to the hemisphere of the target region, while f_2 is mainly assigned to antennas on the opposite side. This imbalance increases the modulation depth at the off-center focus while suppressing unintended amplitude modulation elsewhere, consistent with compensating for the physical and electrical asymmetry introduced by a shifted focal point.

The results of the normalized amplitude modulation depth E_{AM} after TI optimization are shown in Fig. 13 for center focus and in Fig. 14 for side focus. In both cases, a focal region can be observed where intended, with minimal amplitude

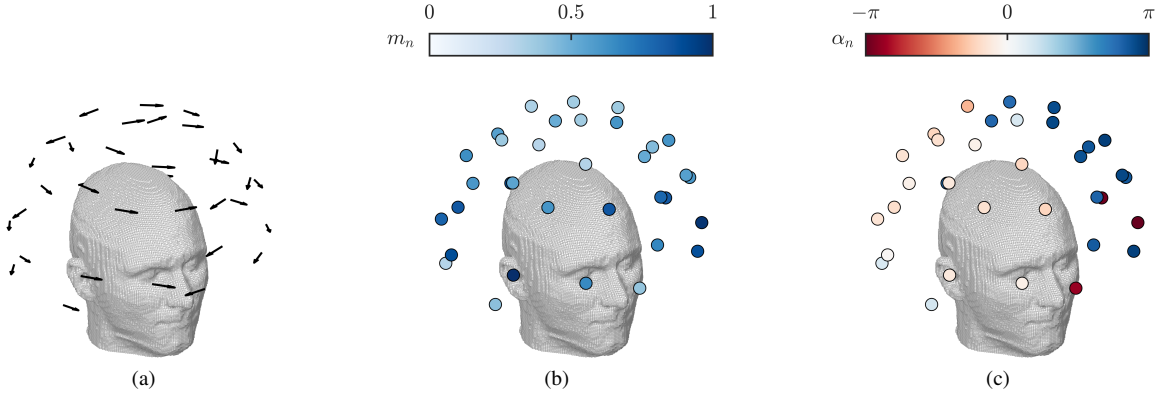


Fig. 9. Array antenna properties showing (a) dipole direction, (b) normalized magnitude m_n , and (c) phase α_n , for each antenna element after iTR optimization for center focus.

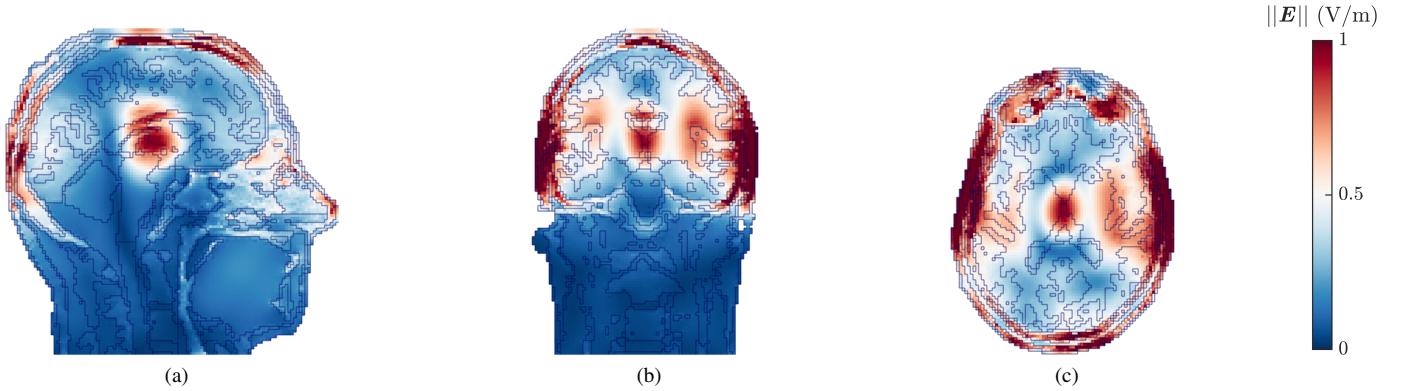


Fig. 10. The resulting norm of the E-field $\|\mathbf{E}\|$ (V/m) for center focus in the (a) sagittal, (b) coronal, and (c) axial plane. The contour outlines represent the discrete interfaces between tissues.

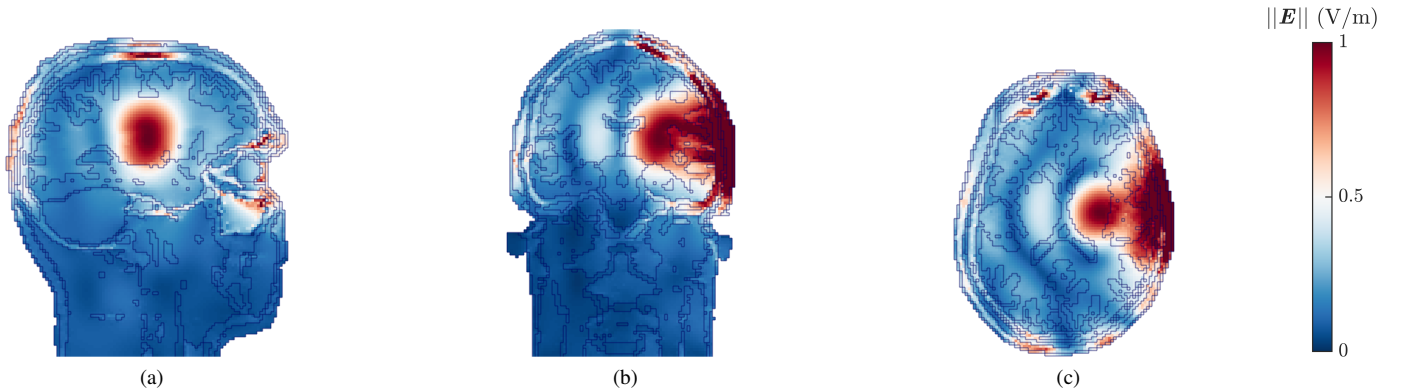


Fig. 11. The resulting norm of the E-field $\|\mathbf{E}\|$ (V/m) for side focus in the (a) sagittal, (b) coronal, and (c) axial plane. The contour outlines represent the discrete interfaces between tissues.

elsewhere. There is some field buildup in the outermost parts of the head, consistent with what was observed in the iTR results.

V. DISCUSSION

This section discusses the results and proposed framework as a two-stage optimization pipeline in which iTR defines the physical characteristics of the array, while TI refines the antenna steering parameters and resulting field distribution to achieve selective neuron stimulation. While iTR and TI are conceptually distinct methods, their combination is essential

for achieving robust and effective performance of the proposed approach.

Using simple radiative sources allows the optimization framework to focus on field shaping, steering, and frequency allocation. This ensures that the performance being evaluated originates from the objective functions and optimization algorithm, rather than from antenna-dependent factors. Accordingly, the results presented in this work should be interpreted as a lower bound on achievable array performance. Further improvements are expected when extending the framework to dedicated antenna designs. These would replace the idealized

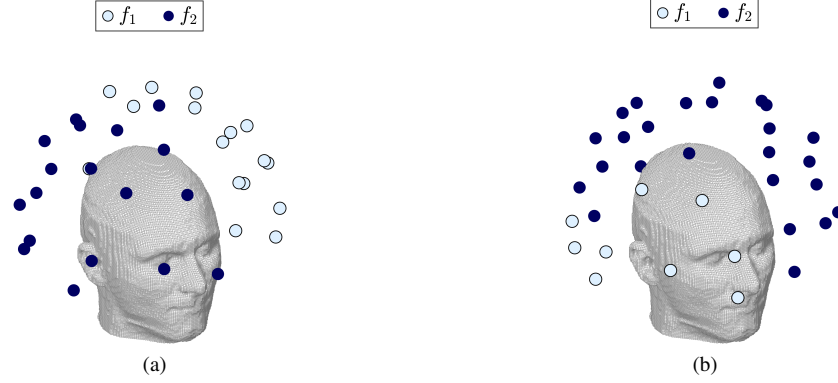


Fig. 12. The resulting split between f_1 and f_2 for (a) center focus and (b) side focus.

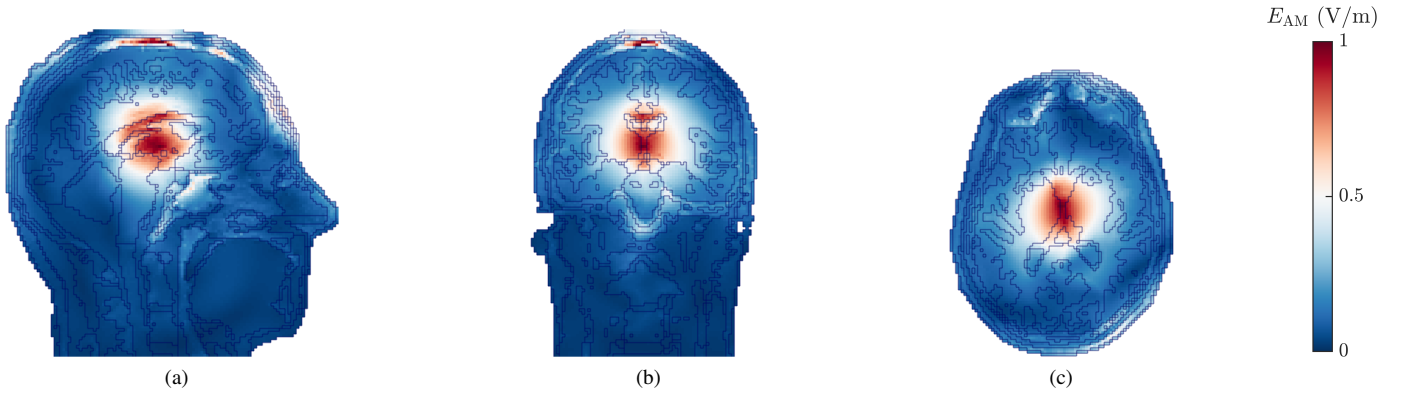


Fig. 13. The resulting amplitude modulation depth E_{AM} (V/m) for center focus in the (a) sagittal, (b) coronal, and (c) axial plane. The contour outlines represent the discrete interfaces between tissues.

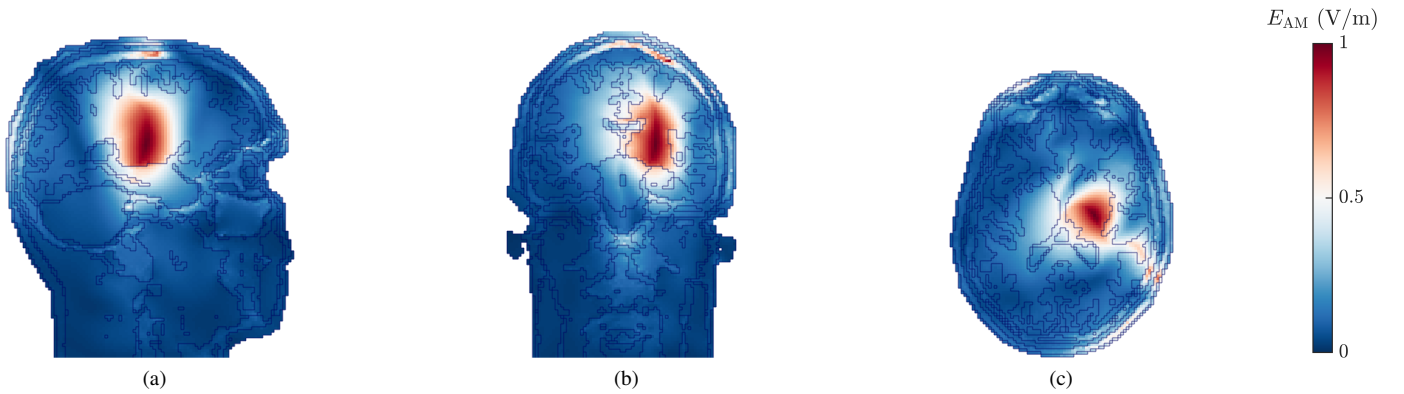


Fig. 14. The resulting amplitude modulation depth E_{AM} (V/m) for side focus in the (a) sagittal, (b) coronal, and (c) axial plane. The contour outlines represent the discrete interfaces between tissues.

MPDs used here with physically realizable antenna elements that offer more directive radiation patterns and are optimized for the operating frequency, array geometry, and near-field interaction with the head tissues.

A. Method-Specific Considerations

1) *Iterative Time Reversal*: It should be noted that in the presented results, the antenna positions act as degrees of freedom, increasing the flexibility of the array design. In this study, candidate antenna positions were restricted to a Fibonacci sphere within the matching layer. For the center-

focus scenario, the focal point is physically equidistant from all potential antenna positions, while the effective electrical path lengths differ due to variations in tissue permittivity along each trajectory. This suggests that alternative antenna configurations could potentially improve the reconstruction of the forward field.

The essential observation from the results in Figs. 10 and 11 is that iTR determines the physical attributes of the array, namely antenna positions and orientations, and provides initial values for the phase and magnitude used in the subsequent TI optimization. Within the proposed two-stage framework,

these results represent an intermediate optimization stage that demonstrates effective focusing of the field distribution within the desired focal regions and yields a reliable initialization for the TI stage.

2) *Temporal Interference*: Building on the field distributions and excitation parameters obtained from iTR, the TI optimization refines the solution toward selective neuron stimulation. The TI optimization produces a well-defined focal region at the intended target location for both center and side focusing, with minimal amplitude elsewhere and only limited field buildup near the outer head regions.

It is important to note that the goal of TI for DBS is to selectively stimulate neurons within a designated brain region. This approach differs fundamentally from hyperthermia aimed at heating tissue. In DBS, the objective is not to raise the temperature at the target region or elsewhere, but to induce neuronal responses. Consequently, high values of the amplitude modulation depth in non-neuronal regions, such as the skull or skin, are of no concern, as these tissues do not respond anyway to the amplitude-modulated field. Therefore, the field evaluation and objective function are defined to specifically reflect the goal of neuronal stimulation, rather than tissue heating as in hyperthermia.

In this work, the objective function \mathcal{J}_{TI} defined in Eq. (19) is used to maximize the envelope amplitude in the target region, effectively focusing the amplitude-modulated field. A natural extension for future studies is to incorporate the orientations of nerve tracts within the target region, since neuronal activation threshold generally is anisotropic [55] with regard to field polarization. In this case, the electric fields could be projected along the known nerve directions [29]. Then, the objective function Eq. (19) can be modified to maximize the envelope amplitude along these directions. Additionally, modulation depth could be further enhanced by including constraints as in [44], or by normalizing the fields so that their contributions are equal at the focal point in each iteration.

The method presented in this study ensures selectivity in the stimulated region, but does not directly consider the field intensity, which is related to tissue energy absorption. A possible extension is to adopt a multi-objective optimization framework, such as a multi-objective genetic algorithm (MOGA) [35], [56], [57]. The ultimate goal of the array is to achieve a high envelope amplitude at the desired focal point while minimizing energy absorption. These objectives may be partially conflicting, and MOGA is well-suited to choose the best trade-off between them along the Pareto front, enabling the selection of solutions that balance stimulation efficacy and patient safety.

B. Combination of iTR and TI

Although iTR and TI can be considered independently, their interaction within the proposed two-stage framework is important for the overall performance. As a potential improvement, an additional optimization step could be introduced between iTR and the TI algorithm. Since the methods are independent, such an intermediate step could provide a refined

initial guess of steering parameters for TI, potentially improving convergence or field focusing. Techniques established in hyperthermia treatment planning could be adopted in this intermediate step to further refine the general field distribution within the focal region.

It should be pointed out, however, that the current results presented in this work indicate that TI optimization already achieves effective focusing with the initial parameters obtained from iTR. Even without the iTR solution for the steering parameters, TI is able to achieve focus of the amplitude-modulated field. This shows that the TI optimization is robust on its own, although convergence is slower and the resulting focus is less precise compared to when TI starts from a well-chosen set of initial parameters.

These observations highlight the role of iTR as an effective initialization stage that improves convergence speed and focal precision, while also demonstrating that the overall framework does not critically depend on perfect combination between the two stages. An intermediate optimization step could still potentially enhance performance, provided that the additional computational cost can be justified.

C. Possible Extensions and Future Development

The presented results were normalized to evaluate the performance of the optimization algorithm in an inhomogeneous head model for focusing of amplitude-modulated fields using TI methods. A continuation could be to use the resulting field distribution as input to single-neuron models to assess what field strengths and spatial distributions are required to achieve single neuron stimulation from TI with MW carrier frequencies. These neurophysiological models describe how electric fields influence voltage-gated ion channels in a single neuron, governing the generation and propagation of action potentials [12].

Neural-network modeling could also be considered. This approach relies on computational or mathematical representations of the structural connectivity between brain regions and provides insight into how focal stimulation effects propagate, as well as how neural circuits and networks respond to electrical input. While electric-field simulations clarify the direct physical effects of non-invasive stimulation, incorporating neuronal orientation and the projections of nerve tracts can be essential for accurately estimating the effective electric fields and their influence on neural pathways [12]. Such modeling can be used to extend the TI objective function to account for axonal orientation, as discussed previously, while also incorporating anisotropic brain tissue properties in simulations to reflect the organization of nerve tracts.

Together, these extensions would enable a closer connection between the optimized electromagnetic fields and the resulting biological responses. This would advance the understanding of the stimulation efficacy and biological effects of the proposed approach for non-invasive DBS.

VI. MEDICAL SAFETY CONSIDERATIONS

Human exposure to EM fields is regulated by international safety standards, most notably the IEEE guidelines [58] and

ICNIRP [59]. These standards define exposure limits to prevent two primary risks: electrostimulation at low frequencies and adverse tissue heating at higher frequencies. Electrostimulation refers to the unintended alteration of neural activity. While this effect is intentionally exploited in therapies such as DBS, it requires exceeding local safety limits within the targeted region. Protection of all off-target tissues remains essential, and the safety standards are designed to ensure that exposures outside the therapeutic region remain well below harmful levels. For head tissues, these limits are expressed mainly in terms of induced electric fields, specific absorption rate (SAR), and allowable temperature rise. Importantly, the thresholds for adverse thermal effects are well above the levels at which meaningful neural modulation is expected to occur.

TI enables the formation of a focused envelope amplitude peak. Following iTR optimization, higher field concentrations may appear in superficial tissues such as skin, skull, and cerebrospinal fluid; these regions contain no neurons and therefore pose no concern for stimulation. Any potential thermal effects in these layers can be mitigated using established hyperthermia techniques, for example, applying a water bolus to cool superficial tissues [60], [61]. Field strengths required for neuronal stimulation are expected to be lower than those used in hyperthermia, consistent with clinically accepted DBS practices, where therapeutic neural activation is achieved without harmful heating.

For MW DBS, the safety requirement is simply to ensure that all amplitude-modulated fields remain below established stimulation thresholds outside the focal region, and that any resulting SAR or thermal increases remain within safety limits throughout the head. In hyperthermia, tissue heating is intentionally produced within a target region while staying below limits elsewhere. Since TI-based neuromodulation aims to avoid heating at the target, meeting these limits is feasible.

VII. CONCLUSION

In this work, we demonstrated that non-invasive microwave temporal interference (TI) fields can be effectively focused within inhomogeneous, realistic head models using external antenna arrays. By combining iterative time-reversal (iTR) for antenna placement and orientation with genetic-algorithm-based TI optimization for frequency, amplitude, and phase assignment, the method achieved high selective amplitude-modulated fields at targeted brain regions, while minimizing off-target modulation. The results highlight the flexibility of the method in steering the focus and its potential to achieve selective and precise neural stimulation.

This study establishes a proof-of-principle for non-invasive, microwave TI-based field modulation and provides a robust method for further development of non-invasive deep brain stimulation systems. Future work could extend the method to incorporate neuronal anisotropy, multi-objective optimization for minimizing off-target energy deposition, and physically realizable antenna designs to further progress towards a clinical non-invasive deep brain stimulation method.

ACKNOWLEDGMENT

The work of M. S. and M. D. was supported by the Swedish Research Council, project number 2023-04887. The work of M. C. and P. N. was supported by the Göran Gustafsson foundation, grant number 2406. We acknowledge R. Nilsson and H. Dobšiček Trefná for discussions and input on the iTR implementation.

REFERENCES

- [1] P. A. Iaizzo, *Introduction to Neurophysiology*. Cham: Springer International Publishing, 2020, pp. 1–64.
- [2] A. M. Lozano, N. Lipsman, H. Bergman, P. Brown, S. Chabardes, J. W. Chang, K. Matthews, C. C. McIntyre, T. E. Schlaepfer, M. Schulder, Y. Temel, J. Volkmann, and J. K. Krauss, “Deep brain stimulation: current challenges and future directions,” *Nat. Rev. Neurol.*, vol. 15, no. 3, pp. 148–160, 2019.
- [3] V. Salanova, “Deep brain stimulation for epilepsy,” *Epilepsy Behav.*, vol. 88, pp. 21–24, Nov. 2018.
- [4] Y. Wu, J. Mo, L. Sui, J. Zhang, W. Hu, C. Zhang, Y. Wang, C. Liu, B. Zhao, X. Wang, K. Zhang, and X. Xie, “Deep brain stimulation in treatment-resistant depression: A systematic review and meta-analysis on efficacy and safety,” *Front. Neurosci.*, vol. 15, Apr. 2021.
- [5] J. K. Krauss, N. Lipsman, T. Aziz, A. Boutet, P. Brown, J. W. Chang, B. Davidson, W. M. Grill, M. I. Hariz, A. Horn, M. Schulder, A. Mammis, P. A. Tass, J. Volkmann, and A. M. Lozano, “Technology of deep brain stimulation: current status and future directions,” *Nat. Rev. Neurol.*, vol. 17, p. 75–87, 2020.
- [6] E. Krames, P. H. Peckham, and A. R. Rezai, *Neuromodulation*, 1st ed. London: Academic Press, 2009.
- [7] P. J. Uhlhaas and W. Singer, “Neural synchrony in brain disorders: Relevance for cognitive dysfunctions and pathophysiology,” *Neuron*, vol. 52, no. 1, pp. 155–168, 2006.
- [8] R. Erzurumlu, G. Sengul, and E. Ulupinar, “Basal ganglia,” in *Human Neuroanatomy*, R. Erzurumlu, G. Sengul, and E. Ulupinar, Eds. Academic Press, 2024, pp. 79–93.
- [9] A. Gunduz, *Deep Brain Stimulation: Emerging Technologies and Applications*. Cham: Springer International Publishing, 2020, pp. 223–243.
- [10] D. Su, H. Chen, W. Hu, Y. Liu, Z. Wang, X. Wang, G. Liu, H. Ma, J. Zhou, and T. Feng, “Frequency-dependent effects of subthalamic deep brain stimulation on motor symptoms in parkinson’s disease: a meta-analysis of controlled trials,” *Sci. Rep.*, vol. 8, no. 1, p. 14456, 2018.
- [11] J. M. Wardlaw, H. Benveniste, and A. Williams, “Cerebral vascular dysfunctions detected in human small vessel disease and implications for preclinical studies,” *Annu. Rev. Physiol.*, vol. 84, no. 1, p. 409–434, Feb. 2022.
- [12] D. Klooster, E. Raaijmakers, M. van Rossum, M. van Beurden, P. Boon, and R. Mestrom, “Non-invasive brain stimulation: from field modeling to neuronal activation,” in *2020 50th Eur. Microwave Conf. (EuMC)*, 2021, pp. 1059–1062.
- [13] L. M. Koponen and A. V. Peterchev, *Transcranial Magnetic Stimulation: Principles and Applications*. Cham: Springer International Publishing, 2020, pp. 245–270.
- [14] D. Q. Truong, N. Khadka, and M. Bikson, *Transcranial Electrical Stimulation*. Cham: Springer International Publishing, 2020, pp. 271–292.
- [15] V. Harid, H. Kim, B.-Z. Li, and T. Lei, “A method for non-destructive microwave focusing for deep brain and tissue stimulation,” *PLoS ONE*, vol. 18, no. 2, p. e0278765, 2023.
- [16] R. Chandra, H. Zhou, I. Balasingham, and R. M. Narayanan, “On the opportunities and challenges in microwave medical sensing and imaging,” *IEEE Trans. Biomed. Eng.*, vol. 62, no. 7, pp. 1667–1682, 2015.
- [17] S. Semenov and D. Corfield, “Microwave tomography for brain imaging: Feasibility assessment for stroke detection,” *Int. J. Antennas Propag.*, vol. 2008, p. 254830, 2008.
- [18] A. Fhager and M. Persson, “Stroke detection and diagnosis with a microwave helmet,” in *2012 6th Eur. Conf. Antennas Propag. (EuCAP)*, 2012, pp. 1796–1798.
- [19] A. Abbosh, “Microwave systems for head imaging: Challenges and recent developments,” in *2013 IEEE MTT-S Int. Microwave Workshop Ser. RF Wireless Technol. Biomed. Healthcare Appl. (IMWS-BIO)*, 2013, pp. 1–3.

- [20] A. T. Mobashsher, K. S. Bialkowski, A. M. Abbosh, and S. Crozier, "Design and experimental evaluation of a non-invasive microwave head imaging system for intracranial haemorrhage detection," *PLoS One*, vol. 11, no. 4, p. e0152351, 04 2016.
- [21] A. Hossain, M. Tariqul Islam, A. Hoque, S. Kamal Abdul Rahim, A. S. Alshammari, M. E. Chowdhury, and M. S. Soliman, "Sensor-based microwave brain imaging system (smbis): An experimental six-layered tissue based human head phantom model for brain tumor diagnosis using electromagnetic signals," *Eng. Sci. Technol., Int. J.*, vol. 45, p. 101491, 2023.
- [22] M. Zanolli and H. Dobsicek Trefna, "Iterative time-reversal for multi-frequency hyperthermia," *Phys. Med. Biol.*, vol. 66, no. 4, p. 045015, 2021.
- [23] D. B. Rodrigues, J. Ellsworth, and P. Turner, "Feasibility of heating brain tumors using a 915 MHz annular phased-array," *IEEE Antennas Wireless Propag. Lett.*, vol. 20, no. 4, p. 423–427, Apr. 2021.
- [24] M. Zanolli, E. Ek, and H. Dobsicek Trefna, "Antenna arrangement in UWB helmet brain applicators for deep microwave hyperthermia," *Cancers*, vol. 15, no. 5, p. 1447, 2023.
- [25] M. Firuzalizadeh, R. Gaffoglio, G. Giordanengo, M. Righero, M. Zucchi, G. Musacchio Adorisio, A. Bellone, A. Vallan, G. Perrone, and G. Vecchi, "Joint optimization of antenna system matching and specific absorption rate focusing in microwave hyperthermia cancer treatment," *Cancers*, vol. 17, no. 3, p. 386, Jan. 2025.
- [26] F. E. S. Pereira, S. K. Jagatheesurumal, S. R. Benjamin, P. C. do Nascimento Filho, F. T. Duarte, and V. H. C. de Albuquerque, "Advancements in non-invasive microwave brain stimulation: A comprehensive survey," *Phys. Life Rev.*, vol. 48, pp. 132–161, 2024.
- [27] B. Hutcheon and Y. Yarom, "Resonance, oscillation and the intrinsic frequency preferences of neurons," *Trends Neurosci.*, vol. 23, no. 5, pp. 216–222, 2000.
- [28] G. Buzsáki, C. A. Anastassiou, and C. Koch, "The origin of extracellular fields and currents — EEG, ECoG, LFP and spikes," *Nat. Rev. Neurosci.*, vol. 13, no. 6, p. 407–420, May 2012.
- [29] N. Grossman, D. Bono, N. Dedic, S. B. Kodandaramaiah, A. Rudenko, H.-J. Suk, A. M. Cassara, E. Neufeld, N. Kuster, L.-H. Tsai, A. Pascual-Leone, and E. S. Boyden, "Noninvasive deep brain stimulation via temporally interfering electric fields," *Cell*, vol. 169, no. 6, pp. 1029–1041.e16, 2017.
- [30] M. A. Safar and R. W. Newcomb, "A system of hemispherical antenna arrays for noninvasive deep brain stimulation," *Math. Probl. Eng.*, vol. 2023, p. 8019934, 2023.
- [31] W. Lee, P. Faeghi, A. D. Dorval, and J. S. Walling, "Wireless beamforming for electromagnetic field focusing in brain tissue," in *2024 54th Eur. Microwave Conf. (EuMC)*, 2024, pp. 489–492.
- [32] A. Madannejad, S. Sadeghi, J. EbrahimiZadeh, F. Ravanbakhsh, M. D. Perez, and R. Augustine, "Microwave beamforming for non-invasive brain stimulation," in *2020 IEEE MTT-S Int. Microwave Biomed. Conf. (IMBioC)*. IEEE, Dec. 2020, p. 1–4.
- [33] M. Seebass, R. Beck, J. Gellermann, J. Nadobny, and P. Wust, "Electromagnetic phased arrays for regional hyperthermia: optimal frequency and antenna arrangement," *Int. J. Hyperthermia*, vol. 17, no. 4, p. 321–336, Jul. 2001.
- [34] H. Elkayal and N. Ismail, "Efficient focusing of microwave hyperthermia for small deep-seated breast tumors treatment using particle swarm optimization," *Comput. Methods Biomech. Biomed. Eng.*, vol. 24, no. 9, pp. 985–994, July 2021, epub 2021 Jun 16.
- [35] D. Baskaran and K. Arunachalam, "Implementation of thinned array synthesis in hyperthermia treatment planning of 434 MHz phased array breast applicator using genetic algorithm," *IEEE J. Electromagn., RF Microw. Med. Biol.*, vol. 7, no. 1, pp. 32–38, 2023.
- [36] M. J. Hajiahmadi, R. Faraji-Dana, and C. Caloz, "Metasurface-based time-reversal focusing for brain tumor microwave hyperthermia," *IEEE Trans. Antennas Propag.*, vol. 70, no. 12, p. 12237–12246, Dec. 2022.
- [37] B. Guo, L. Xu, and J. Li, "Time reversal based microwave hyperthermia treatment of breast cancer," *Microw. Opt. Technol. Lett.*, vol. 47, no. 4, p. 335–338, 2005.
- [38] J. de Rosny, G. Lerosey, A. Tourin, and M. Fink, "Time reversal of electromagnetic waves," in *Modeling and Computations in Electromagnetics*, H. Ammari, Ed. Berlin, Heidelberg: Springer Berlin Heidelberg, 2008, pp. 187–202.
- [39] M.-C. Gosselin, E. Neufeld, H. Moser, E. Huber, S. Farcito, L. Gerber, M. Jedensjö, I. Hilber, F. D. Gennaro, B. Lloyd, E. Cherubini, D. Szczerba, W. Kainz, and N. Kuster, "Development of a new generation of high-resolution anatomical models for medical device evaluation: the virtual population 3.0," *Phys. Med. Biol.*, vol. 59, no. 18, pp. 5287–5303, 2014.
- [40] COMSOL AB, "Comsol multiphysics," Stockholm, Sweden, 2025. [Online]. Available: <https://www.comsol.com>
- [41] The MathWorks, Inc., "Matlab," Natick, MA, USA, 2024. [Online]. Available: <https://www.mathworks.com>
- [42] J. de Rosny, G. Lerosey, and M. Fink, "Theory of electromagnetic time-reversal mirrors," *IEEE Trans. Antennas Propag.*, vol. 58, no. 10, pp. 3139–3149, 2010.
- [43] The MathWorks, Inc., "bayesopt (Bayesian Optimization)," Natick, MA, USA, 2025, accessed: Jun. 6, 2025. [Online]. Available: <https://www.mathworks.com/help/stats/bayesopt.html>
- [44] F. Ahsan, T. Chi, R. Cho, S. A. Sheth, W. Goodman, and B. Aazhang, "Emvelop stimulation: minimally invasive deep brain stimulation using temporally interfering electromagnetic waves," *J. Neural Eng.*, vol. 19, no. 4, p. 046005, Jul. 2022.
- [45] S. M. Bawin, L. K. Kaczmarek, and W. R. Adey, "Effects of modulated VHF fields on the central nervous system," *Ann. N. Y. Acad. Sci.*, vol. 247, no. 1, p. 74–81, Feb. 1975.
- [46] R. C. Beason and P. Semm, "Responses of neurons to an amplitude modulated microwave stimulus," *Neurosci. Lett.*, vol. 333, no. 3, p. 175–178, Nov. 2002.
- [47] F. Ahsan, A. C. Govindaraju, R. M. Raphael, T. Chi, S. A. Sheth, W. Goodman, and B. Aazhang, "Biophysics of amplitude-modulated giga-hertz electromagnetic waves stimulation," in *2023 57th Asilomar Conf. Signals, Syst., Comput.* IEEE, Oct. 2023, p. 1463–1468.
- [48] The MathWorks, Inc., "Genetic algorithm and direct search toolbox: GA Function," Natick, MA, USA, 2025, accessed: Jul. 22, 2025. [Online]. Available: <https://se.mathworks.com/help/gads/ga.html>
- [49] J. Redr, T. Pokorný, T. Drizdal, O. Fiser, M. Brunat, J. Vrba, and D. Vrba, "Microwave hyperthermia of brain tumors: A 2d assessment parametric numerical study," *Sensors*, vol. 22, no. 16, p. 6115, 2022.
- [50] C. Lyu, W. Li, and B. Yang, "Differential evolution optimization of microwave focused hyperthermia phased array excitation for targeted breast cancer heating," *Sensors*, vol. 23, no. 8, 2023.
- [51] IT'IS Foundation, "Foundation for research on information technologies in society," 1999, accessed: Aug. 2025. [Online]. Available: <https://itis.swiss/>
- [52] ———, "Tissue Properties Database," 2018, version V4.0.
- [53] W. R. Hendee and E. R. Ritenour, *Medical Imaging Physics*. Wiley-Liss, 2002.
- [54] M. Ghaderi Aram, M. Zanolli, H. Nordström, I. Toma-Dasu, K. Blomgren, and H. Dobšiček Trefná, "Radiobiological evaluation of combined gamma knife radiosurgery and hyperthermia for pediatric neuro-oncology," *Cancers*, vol. 13, no. 13, p. 3277, Jun. 2021.
- [55] L. Wu, A. Cannà, O. Narvaez, J. Ma, S. Sang, L. J. Lehto, A. Sierra, H. Tanila, Y. Zhang, O. Gröhn, W. C. Low, P. Filip, S. Mangia, and S. Michaeli, "Orientation selective DBS of entorhinal cortex and medial septal nucleus modulates activity of rat brain areas involved in memory and cognition," *Sci. Rep.*, vol. 12, no. 1, p. 8565, 2022.
- [56] A. Konak, D. W. Coit, and A. E. Smith, "Multi-objective optimization using genetic algorithms: A tutorial," *Reliab. Eng. Syst. Saf.*, vol. 91, no. 9, pp. 992–1007, 2006, special Issue - Genetic Algorithms and Reliability.
- [57] MathWorks, "gamultiobj – find pareto front of multiple fitness functions using genetic algorithm," <https://se.mathworks.com/help/gads/gamultiobj.html>, 2025, accessed: 2025-08-14.
- [58] *IEEE Standard for Safety Levels with Respect to Human Exposure to Electric, Magnetic, and Electromagnetic Fields, 0 Hz to 300 GHz*, IEEE Std. IEEE Std C95.1-2019, 2019.
- [59] International Commission on Non-Ionizing Radiation Protection, "Guidelines for limiting exposure to electromagnetic fields (100 kHz to 300 GHz)," *Health Phys.*, vol. 118, no. 5, p. 483–524, May 2020.
- [60] T. Drizdal, G. C. van Rhooen, R. F. Verhaart, O. Fiser, and M. M. Paulides, "A guide for water bolus temperature selection for semi-deep head and neck hyperthermia treatments using the hypercollar3d applicator," *Cancers*, vol. 13, no. 23, p. 6126, Dec. 2021.
- [61] R. G. et al., "Fast optimization of temperature focusing in hyperthermia treatment of sub-superficial tumors," 2020, arXiv:2006.13261.